

## THE EVOLUTION OF THE PLANETARY NEBULA NGC 6826

PHILIP PLAIT

Department of Astronomy, University of Virginia, Charlottesville, Virginia 22903

NOAM SOKER

Harvard-Smithsonian Center for Astrophysics, Mail Stop 15, 60 Garden Street, Cambridge, Massachusetts 02138

*Received 20 January 1990; revised 20 February 1990*

## ABSTRACT

The density and mass profiles of the planetary nebula NGC 6826 are studied. New CCD images are used to deconvolve the density from the emission measure in  $H\alpha$ , assuming that the planetary nebula is spherically symmetric. For an assumed distance of 1.54 kpc the mass of the inner region  $r < 13$  arcsec is  $\sim 0.15 M_{\odot}$  and that the entire visible planetary nebula is  $0.54 M_{\odot}$ . The possible formation of the dense shell at the edge of the nebula as a result of interaction with the ISM is discussed. The formation of the spherical outer halo together with an elliptical inner region can be explained by a low mass companion to the progenitor of NGC 6826 that was evaporated or collided with the central star.

## I. INTRODUCTION

Planetary nebulae (PNs) received much attention in the last decade, partially as a result of *IUE* observations of fast winds from central star of PNs e.g., Perinoto 1989; Torres-Peimbert 1989) and from new CCD images of PNs (e.g., Balick 1987), which gave a better understanding of their evolution. Balick (1987) discusses and suggests morphology and evolutionary classification for PNs, which he claims is in agreement with the interacting winds model of PNs. In this model, the hot central star of the PN emits a low-density fast wind at a velocity of  $\sim 1000$  km s $^{-1}$ . This fast wind "catches up" with the slow wind resulting from the ejection of the progenitor red giant's envelope (moving at  $\sim 10$  km s $^{-1}$ ) and drives a shock wave into it (Kwok, Purton, and Fitzgerald 1978; Kwok 1982; Volk and Kwok 1985). Axisymmetrical numerical simulations show that the interacting winds model can explain the basic morphology of elliptical PNs (Soker and Livio 1989), although they cannot explain the "ansae" (Soker 1990). The ansae (see Balick 1987) are two bright knots on opposite sides of the central star along the major axis found in some elliptical PNs.

For better understanding of the mechanisms that shape PNs, among other things, more detailed density and velocity profiles of PNs are needed. In this paper we study the density profile of the elliptical PN NGC 6826. This is a well-studied PN with a detailed optical map given by Balick (1987) and Jacoby, Quigley, and Africano (1987). As can be seen very clearly in Balick (1987), NGC 6826 contains two distinct regions: a bright inner region extending to a radius of  $\sim 13$  arcsec, and a faint halo extending from the inner region up to  $\sim 70$  arcsec from the central star. The inner region (also called the core) can be divided into four main regions; a very low surface-brightness inner region, a bright elliptical rim, a bright axisymmetrical shell surrounding the rim, and two ansae along the major axis but outside of the rim. The faint halo is somewhat filamentary with a bright shell at its outer edge (Middlemass, Clegg, and Walsh 1989). Hippelein, Baessgen, and Grewing, (1985), Manchado and Pottasch (1989), and Middlemass *et al.* (1989) find the halo to be  $\sim 2$  to  $\sim 3$  times more massive than the inner region. The halo temperature is higher than that of the inner region and its metal abundances are lower than that of the inner region

(Manchado and Pottasch 1989; Middlemass *et al.*, 1989). A velocity map for the inner region is given in Balick, Preston, and Icke (1987) and the expansion velocity of the halo is found by Hippelein *et al.* (1985) to be 6 km s $^{-1}$ .

With new CCD images of NGC 6826 (Sec. II) we give density and mass profiles (Sec. III) and discuss the interaction of the PN halo with the ISM (Sec. IV) and its evolution (Sec. V).

## II. OBSERVATIONS

*a) Instrumentation*

The observations were taken over a period of four days (28 August 1989) at the University of Virginia Fan Mountain Observatory. The telescope is a 1 m Cassegrain equipped with a Photometrics 3000 series CCD camera which contains a Thompson 7882 CDA CCD chip. The chip is front illuminated and was kept at a constant temperature of  $-120$  °C throughout the observing run. The pixels are  $23 \mu\text{m}$  corresponding to 0.352 arcsec at the focal plane of the telescope. The format size is  $384 \times 576$  pixels, giving a field of view of  $135.1 \times 202.7$  arcsec. 1 ADU (Analog Digital Unit) corresponds to 16.75 photons.

*b) Observations*

The nebula was observed in two bandpasses:  $H\alpha$  and an adjacent band. The filters were centered on 6575 and 6645 Å, respectively. The continuum filter contained no or only weak nebular lines. Both filters have a FWHM of 70 Å.

The seeing was steady at approximately 2 arcsec on all the nights and the transparency was excellent. The nebula was observed only when it was within 2 hr of the meridian.

The  $H\alpha$  filter has a flaw in it that produces a secondary "ghost" image 54 pixels north and 17 pixels east from the primary image (see Fig. 1), adding a systematic noise to the data. This ghost image is almost certainly due to an external reflection in the filter. None of the other filters display such a secondary image. Analysis using the central star of NGC 6826 and  $\beta$  Cygni (Albireo) showed that the intensity of the image is approximately 0.006 times that of the primary image. To determine the extent of the error, a circular mask of

radius 12 arcsec was placed over the ghost image. The reduction programs then ignored the masked area (Sec. II *d*). It was found that the ghost image added a maximum of  $\sim 30\%$  of the density of the affected region, although the average error is smaller. The change in total mass of the nebula due to the ghost image is  $< 3\%$ . The final analysis of the nebula was done with the ghost image masked in this way.

### c) Image Reduction

Four images over three nights were used in making the final  $H\alpha$  image, while three images over three nights were used in making the continuum image. Each integration was 30 min long.

The raw images were reduced using the IDL (Interactive Data Language) software package on a Micro Vax. The domeflats in both filters unfortunately suffered from edge darkening due to uneven illumination of the dome area, but this problem was alleviated by median filtering. Due to a software problem in the CCD controller, some of the biases were unstable, so the good biases over all the applicable nights were averaged to get a master bias for all nights. This process yielded a good bias since the chip was very stable over the run. The images were then divided by the domeflats and had the biases subtracted in the usual way.

Once the individual images were reduced, they were centered by determining the coordinates of the central star in each image and then shifting the images so that the central stars coincided. A vertical white line was produced in the final image due to the shifted edge of one of the  $H\alpha$  images. Since the line is at the extreme edge of the nebula, it did not interfere with the reductions.

Unfortunately, the nebula's faint outer halo is slightly larger than the field of view of the chip, so there was a small loss of information about the northern and southern portions of the nebula. The loss, however, was small and did not significantly affect the reductions.

The four centered  $H\alpha$  images were averaged to produce a final  $H\alpha$  image while the three continuum images were median filtered. At this point cosmic rays were rejected by replacing the affected pixels with an average background value near the hit. The final image was then produced by subtracting the continuum image from the  $H\alpha$  image. No scaling was needed as the observations were of the same time, under the same conditions, and the background value went to zero (within the noise) after subtraction without scaling. The final  $H\alpha$  image of NGC 6826 is given in Fig. 1 [Plate 98].

### d) Data Analysis

The goal of the data reduction was to produce a radial profile of the emission measure of the nebula. The outer halo has a very low surface brightness, thus pixel binning was required to obtain a good signal-to-noise ratio. To do this, we assumed azimuthal symmetry and binned pixels in concentric annuli.

The faint outer halo is fairly symmetric azimuthally. There are numerous indentations along the rim, discussed in Sec. IV. In general, these deviations from azimuthal symmetry are quite small, on the order of a few arcseconds. There is one region in the northeast part of the outer halo which contains a large concavity with a brighter than average blob (as it appears on the image). As a check, the data were analyzed with this blob masked and unmasked. No significant difference was found, and thus the blob was left in. The stars in the regions of interest were masked by circular areas, and the reduction programs skipped over these regions in the analysis.

The radial emission measure profile (Fig. 2; we assume that the conditions are the same in the whole nebula, so that the emission measure is proportional to the ADU value) was obtained by defining a series of concentric annuli around the center of the nebula (taken to be at the central star) and

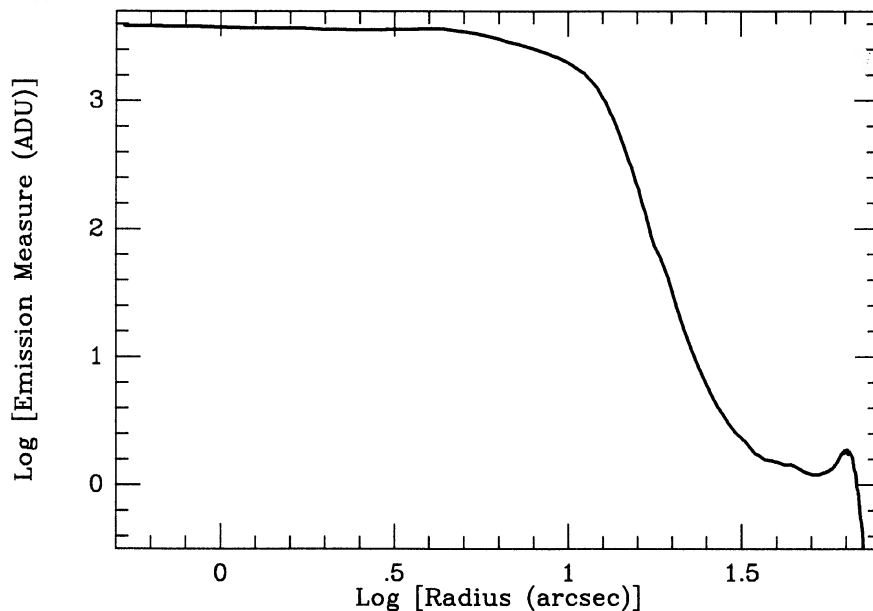


FIG. 2. The  $H\alpha$  emission measure vs radius of NGC 6826.

averaging the pixel values in each annulus. For the inner, brighter regions, averaging was done over a one pixel increment in the radial direction. In the fainter halo region, averaging was done over five pixels radially. Although this reduced spatial resolution, it greatly enhanced the signal-to-noise ratio. For the region near the edge of the nebula, averaging was again done over one pixel increments in order to resolve spatially the edge of the halo. Initially, the profile was determined to a distance of 215 pixels (75.7 arcsec) from the center of the nebula. This was done to get well past the edge of the outer halo and into the background noise, to determine where the information about the nebula is lost in the noise. We found that the last information with a good signal-to-noise ratio is at a distance of 201 pixels (71 arcsec) from the center of the nebula. The background level did not quite go to zero; it approached a value of approximately 0.15 ADU. This value was then subtracted from the values previously found for the nebula.

### III. THE DENSITY PROFILE OF NGC 6826

The density profile of the nebula was determined by deconvolving the density from the emission measure in  $H\alpha$  using an Abel's Integral Equation and assuming spherical symmetry. These can give nonaccurate density and mass determinations for the inner regions for two reasons. First, the inner region is far from being spherically symmetric, and second, near the ansae the intensity of  $[N II]$  (6548 + 6583) is 20% of that in  $H\alpha$ , compared to only 3.6% when averaged over the nebula (Balick, private communication). A small inaccuracy in the density determination in the halo is introduced by the weak filamentary structure imposed on the generally smooth halo. It was also assumed that the center of the nebula was coincident with the central star. The CCD only provides a determination of the emission measure to an arbitrary constant. This constant depends on the scaling of the ADU of the chip. Absolute photometry needs to be done to scale the data. Thus the profile was scaled such that the

electron density at a distance of 12 arcsec from the center was  $1000 \text{ cm}^{-3}$  (Jacoby *et al.* 1987; Barker 1988).

The density profile is presented in Fig. 3. The bright peak at the center corresponds to the central star. The small peak adjacent to the central star is a remnant of the image reduction process and therefore is not real. The dip at 3 arcsec is due to an evacuated region between the central star and the rim. The second peak at 5 arcsec from the center is due to the rim. The rim is elliptical in shape and this is smoothed somewhat in the density profile because of the azimuthal averaging. The broad shallow slope around 12 arcsec from the center is due to the two ansae on either side of the central star. They are relatively large features roughly equidistant from the center and thus are not sharply peaked on the profile.

Outside of the ansae the density drops smoothly in the inner region out to  $\sim 12.5$  arcsec. Here there is a change of slope in the graph as the emission becomes dominated by the faint outer halo. The density falls smoothly once again until 60 arcsec from the center, where the effect of the compression of the edge of the outer halo can be seen. This is seen better in Fig. 4, which includes only the outer region of the nebula.

When the density profile is graphed on a log-log plot (Fig. 5), a clear power law drop in density,  $n_e \propto r^{-\alpha}$  with  $\alpha \approx 4$ , from 13 to 37 arcsec (1.11–1.57 on the scale of the graph) can be seen. A freely expanding wind with constant velocity and mass-loss rate would follow an  $\alpha = 2$  power law. We therefore conclude that the mass-loss rate increased very strongly with time during this period, assuming that the velocity did not change by much. The density profile from 37 to 58 arcsec can be described roughly by an  $\alpha = 1.6$  power law. This shallow density profile can result from an interaction with surrounding material, as we discuss in the next section.

The mass density of the nebula was determined by assuming that helium is singly ionized (Manchado and Pottasch 1989). A distance to the nebula of 1.54 kpc was used (Balick 1987), yielding a nebular radius of 0.53 pc. The mass interior

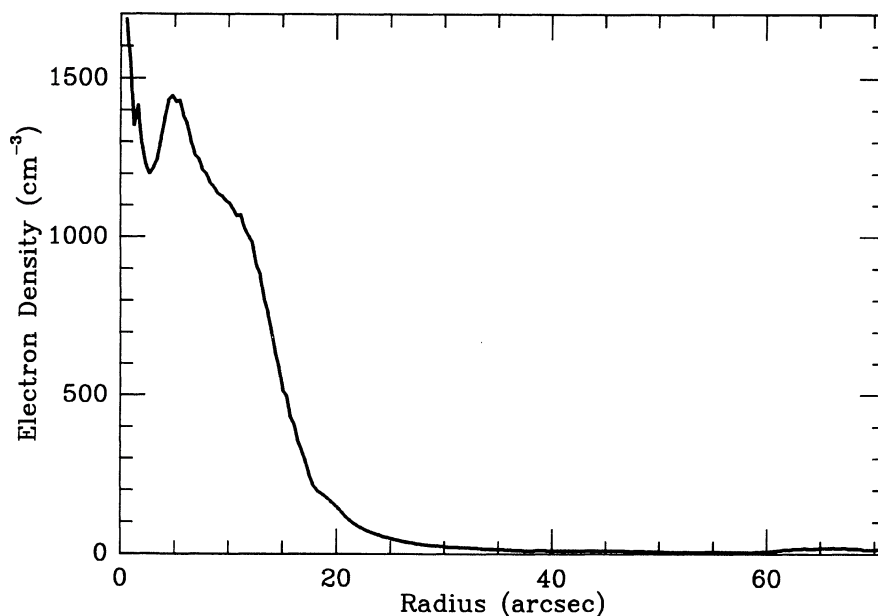


FIG. 3. The density profile of NGC 6826, deconvolved from the emission measure. The plot was scaled so that the density at 12 arcsec is  $1000 \text{ cm}^{-3}$ .

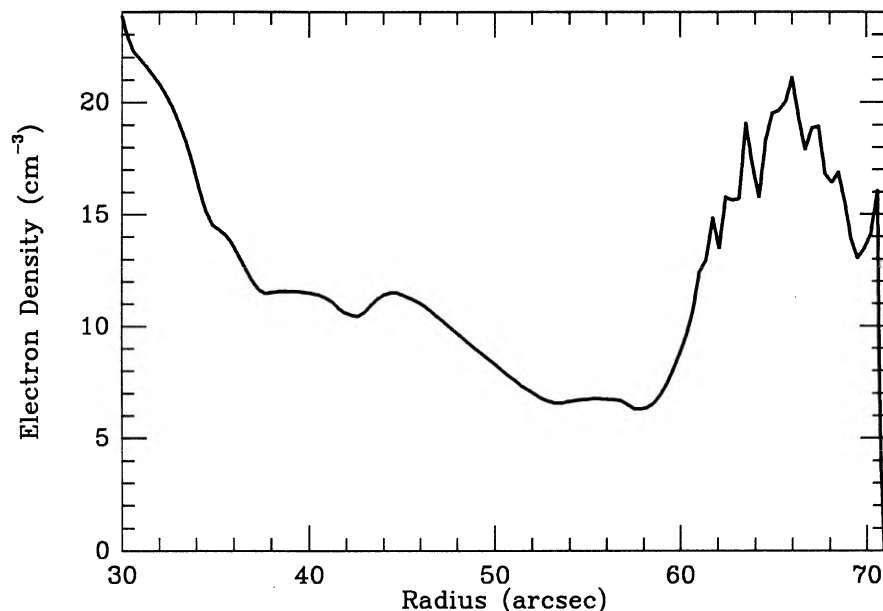


FIG. 4. The density profile of NGC 6826, concentrating on the edge of the outer halo. The spatial resolution of the edge was traded for noise in the signal.

to a radius versus that radius is plotted in Fig. 6. The slope change at a radius of  $\sim 0.12$  pc is due to the density drop from the inner to the outer halo. The volume increases rapidly enough so that the drop in density is more than compensated by the total mass of the nebular material in the faint outer halo. The slope increase at a radius of  $\sim 0.45$  pc is due to the high density shell at the edge of the halo.

We find the mass of the inner region  $r < 13$  arcsec to be  $\sim 0.15 M_{\odot}$  and the total mass to be  $0.54 M_{\odot}$ . Manchado and Pottasch (1989) find, for an assumed distance of 1 kpc, these masses to be 0.06 and  $0.17 M_{\odot}$ , respectively, and Hippelein *et al.* (1985) 0.06 and  $0.25 M_{\odot}$ , for an assumed distance of 1.02 kpc. Although they did not resolve the density profile, but rather used extra assumptions concerning the

nebula, the agreement in the inner region to halo mass ratio is good. Absolute masses depend strongly on assumed distance to the nebula. Thus, for example, if we had taken the distance to be 1 kpc, as these papers did, we would find the total mass to be  $\sim 0.15 M_{\odot}$ . We want to stress again that the inner region has an elliptical shape and contains the ansae, so that the assumption of spherical symmetry can introduce an error in the density and mass determinations of this region.

#### IV. INTERACTION WITH AN EXTERNAL MEDIUM

The sharp edge of the halo observed in several PNs can be explained by a ram pressure deceleration of the expanding halo by an external medium (Balick, private communica-

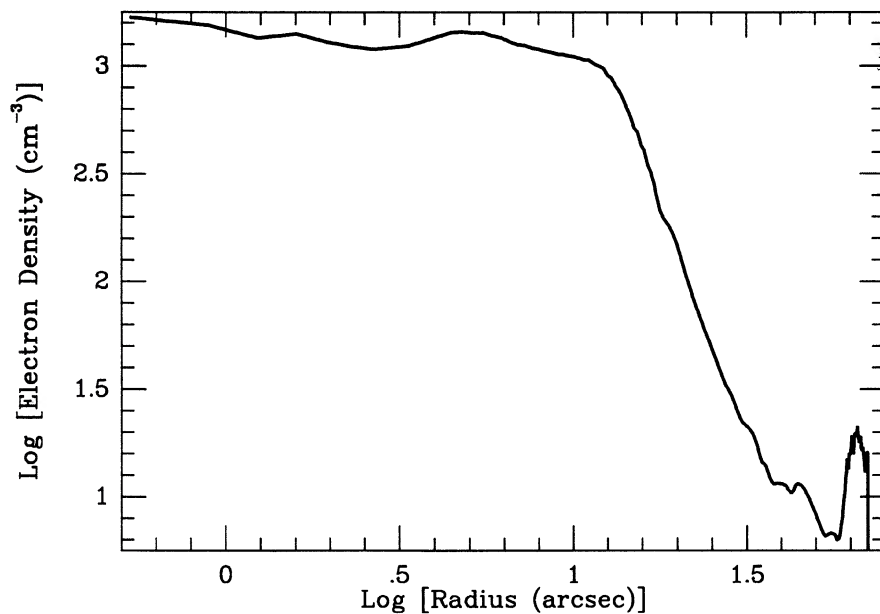


FIG. 5. The density profile of NGC 6826 plotted in log space. Here the  $\alpha = -4$  power law drop of the faint outer halo is most apparent.

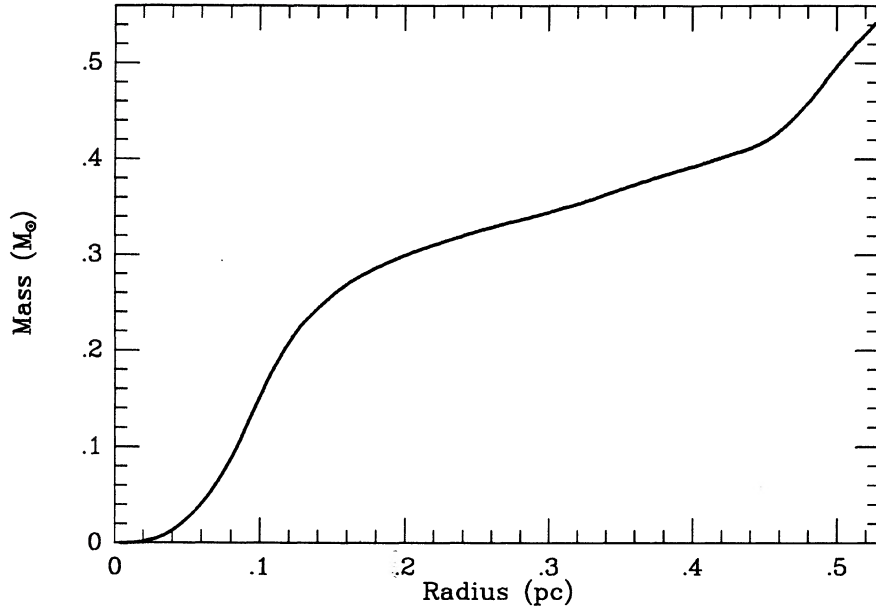


FIG. 6. The mass interior to a radius as function of that radius assuming a distance of 1.54 kpc.

tion). When the density of the halo becomes very low, even a small velocity of the PN relative to the ISM will deform the shell substantially (Borkowski, Sarazin, and Soker 1990). In an intermediate stage, a thin shell can be formed. Such a shell can be observed at the edge of the faint halo of NGC 6826 (see Figs. 1 and 4). We show here that under a few simplified assumptions a crude estimate of the properties of the halo and ISM (or circumstellar medium) around NGC 6826 can be made, if the shell is a result of a halo-ISM interaction. The geometry is drawn schematically in Fig. 7. The expansion velocity, density, and temperature in the undisturbed region  $r < r_a$  are  $v_1$ ,  $\rho_1$ , and  $T_1$ , respectively. The flow in this region is assumed to be supersonic,  $M = v_1/\sqrt{\Theta_1} > 1.3$ , where  $M$  is the isothermal mach number of the halo and  $\Theta \equiv kT/\mu m_p$ , with the usual meaning of the symbols. We assume that the shell is thin,  $r_b - r_a \ll r_a$ , with density  $\rho_2$ , velocity  $v_2$  and

temperature  $T_2 = T_1$ . The density and temperature of the ISM are  $\rho_I$  and  $T_I$ , respectively. We assume that the shell evolves slowly, which means that a pressure equilibrium exists in both sides of the shell. This is the case as long as the mass in the shell  $\mathcal{M}_2$  is small compared to  $4\pi\rho_1 r_2^3$ , so that the term  $\mathcal{M}_2 dv_2/dt$  can be neglected in the momentum equation, and if the shell was not heated recently. The radius of the shell is taken to be  $r_2 = (r_a + r_b)/2$ . We will discuss the case where the shell was heated at a late time by the central star radiation later on. Using the assumptions mentioned above, these can be written as,

$$\rho_1[\Theta_1 + (v_1 - v_2)^2] = \rho_2\Theta_2; \quad \rho_1(\Theta_1 + v_2^2) = \rho_2\Theta_2, \quad (1)$$

at  $r_a$  and  $r_b$ , respectively. Eliminating  $\rho_2\Theta_2$  from Eq. (1) gives

$$\rho_1[\Theta_1 + (v_1 - v_2)^2] = \rho_1(\Theta_1 + v_2^2). \quad (2)$$

Such a shell can be formed only when

$$\rho_1\Theta_1 \leq \rho_I(\Theta_1 + v_1^2). \quad (3)$$

The radius at which the equality occurs in Eq. (3) is marked  $r_0$  and the time is set to  $t = 0$ . Before that time the ISM decelerates the expanding halo, but a shallow pressure and density gradient is formed in the halo, rather than a shell. We do not treat this process here. We further assume that  $n_I \ll n_1$  and neglect terms of order  $n_I/n_1$ , and that the density in the halo changes as  $r_2^{-2}$  as the shell expands. Solving for  $v_2$  from Eq. (2) gives the equation for the position of the shell  $r_2$ ,

$$\dot{r}_2 \equiv v_2 = v_1 - \sqrt{\Theta_1} \sqrt{\left(\frac{r_2}{r_0}\right)^2 - 1}. \quad (4)$$

For small values of  $Y$  the solution for the velocity and position of the shell can be expanded into a series

$$\frac{v_2}{v_1} = 1 - Y + \frac{1}{3}Y^2 - \frac{1}{8}\left(M^2 + \frac{2}{9}\right)Y^3 + O(Y^4), \quad (5)$$

and

$$r_2 = r_0 + v_1 t \left[ 1 - \frac{3}{2}Y + \frac{1}{6}Y^2 - \frac{1}{20}\left(M^2 + \frac{2}{9}\right)Y^3 + O(Y^4) \right], \quad (6)$$

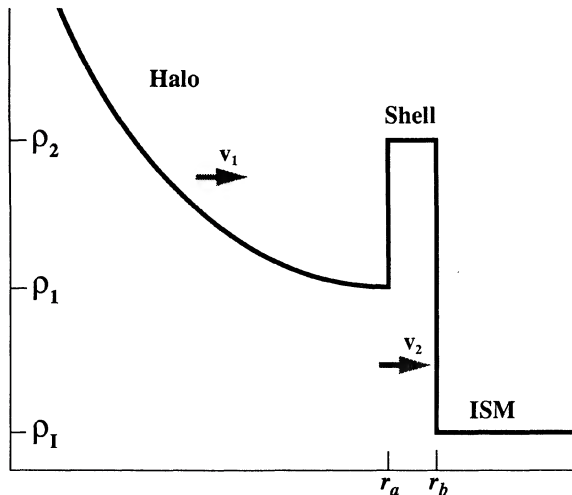


FIG. 7. A schematic density profile of a shell at the edge of an outer halo.

respectively, where

$$Y \equiv \sqrt{\frac{2}{M^2} \frac{v_1 t}{r_0}} \quad (7)$$

If the density profile in the halo near the shell is taken to be  $\rho = \rho_a (r_a/r)^\alpha$ , the total mass in the shell is given by

$$\begin{aligned} \mathcal{M}_2 &= \int_{r_a}^{r_0 + v_1 t} 4\pi \rho_a (r_a/r)^\alpha r^2 dr \\ &= \frac{4\pi}{3-\alpha} \rho_a r_a^3 \left[ \left( \frac{r_0 + v_1 t}{r_a} \right)^{3-\alpha} - 1 \right]. \end{aligned} \quad (8)$$

If  $\mathcal{M}_2/(\rho_a r_a^3)$  is known, we can eliminate  $v_1 t$  from Eqs. (6) and (8) and solve for  $r_0$  and  $Y$  as a function of  $M$ . We can then find  $v_2/v_1$  from (5), and since  $\rho_2/\rho_1$  is assumed to be known, a unique value for  $M$  and  $v_2/v_1$  can be found from the first equation in (1), which can be written as

$$\rho_2/\rho_1 = 1 + M^2(1 - v_2/v_1)^2. \quad (9)$$

For NGC 6826 we take the following parameters:  $r_2 = 66$  arcsec,  $r_a = 60$  arcsec,  $n_e(r_a) = 5 \text{ cm}^{-3}$ ,  $\mathcal{M}_2 = 0.125 \mathcal{M}_\odot$  and  $\alpha = 1.6$ . Solving by iteration for  $r_0$  and  $Y$  from Eqs. (6) and (8), and taking  $\rho_2/\rho_1 = 4$  we find  $M \simeq 2$ ,  $r_0 \simeq 0.3$  pc and  $v_2/v_1 \simeq 0.1$ .

The small velocity of the shell  $v_2/v_1 \ll 1$ , means that the shell expansion was almost completely stopped by the ISM pressure. If the temperature of the halo is taken to be  $T_1 = 10^4$  K it follows from Eq. (2) that the pressure of the ISM is  $n_I T_I \sim 2 \times 10^5 \text{ cm}^{-3} \text{ K}$ , where  $n_I$  is the ISM proton number density. This is much above the expected pressure of the ISM at 340 pc above the galactic disk. It is possible that the formation of the shell occurred before the halo was heated by the central star. The existence of dust and molecular gas in some halos of PNs suggests that the temperature can be as low as a few  $\times 100$  K. After the shell was heated by the central star it expanded and its density dropped. If we take the density ratio to be much higher than its current value, say,  $\rho_2/\rho_1 = 15$ , we find  $M \simeq 5$ ,  $r_0 \simeq 0.18$  pc and  $v_2/v_1 \simeq 0.25$ . Taking the velocity of the halo to be  $v_1 = 6 \text{ km s}^{-1}$  (Hippelein *et al.* 1985) and assuming an atomic gas, the temperature of the halo before it was heated was  $T_1 \simeq 350$  K. The pressure of the ISM is found from Eq. (2) to be  $n_I T_I \simeq 7000 \text{ cm}^{-3} \text{ K}$ . This is still much higher than the pressure of the warm medium which has a density of  $n < 0.1 \text{ cm}^{-3}$  at this height above the galactic plane (Lockman 1990). Such a high pressure may result from a hot medium ( $T \sim 10^6$  K) together with a strong magnetic pressure.

The large density fluctuations along the shell suggest that some kind of instability might result from the interaction with the ISM. The process of decelerating a PN shell by a hot medium is unstable against Rayleigh-Taylor instability (Soker, Borkowski, and Sarazin 1990). Since the shell is very cold, this instability might arise even if the ISM is at  $T \sim 10^4$  K.

To summarize, if the shell at the edge of the halo is a result of an interaction with the ISM, the pressure of the ISM should be quite high,  $n_I T_I \sim 10^4 \text{ cm}^{-3} \text{ K}$ , considering that NGC 6826 is 340 pc above the galactic plane. Other possibilities are that the shell is a result of an ionization front, that it interacts with some circumstellar medium or that the shell was ejected during a short period of time. The first alternative seems unfavorable, as it seems that the nebula is mass limited and not ionization limited (Middlemass *et al.* 1989). In the latter alternative the shell would stay thin if the Mach

number of the shell is very high, of the order of the ratio of the radius to half the shell width (ratio  $\sim 10$ ). For  $v_1 = 6 \text{ km s}^{-1}$  the temperature of the shell was then  $\sim 100$  K. A possible mechanism to eject a shell during a short period of time is an interaction with a low mass companion when it enters the progenitor red giant's envelope (see next section). A small problem with this scenario is that, unlike the inner region, the outer halo shows only a weak large-scale asymmetry. A bright thin shell at the edge of the halo can be seen in several PNs (Chu 1989). This might suggest that interaction with circumstellar medium or ejection of the shell is more likely than interaction with ISM having nontypical conditions.

## V. THE FORMATION OF THE ELLIPTICAL INNER HALO

### a) The Common Envelope Scenario for the Formation of Elliptical PNs

A review of several mechanisms for the formation of axisymmetrical PNs is given by Morris (1990). He concludes that the binary star model is the most successful one. Here we will concentrate on the common envelope scenario.

Based on the two-dimensional common envelope numerical simulations of Bodenheimer and Taam (1984) and the three-dimensional numerical simulations of Livio and Soker (1988), Soker and Livio (1989), and Soker (1989) argue that the common envelope is a natural mechanism to produce elliptical PNs. Soker (1990) argues that the angular momentum which is deposited into the red giant (RG) envelope by a moderate companion having a mass of few  $\times 0.1 \mathcal{M}_\odot$ , at an initial separation of few  $\times 10^2 R_\odot$  can lead to the formation of an elliptical PN.

In addition to the "quiet" common envelope phase, there are other, more violent effects that might occur when a secondary is spiralling-in inside the common envelope (Soker 1990). First, a massive companion, or a moderate one when it enters the RG envelope, can cause high-velocity flow of gas in the equatorial plane (Livio and Soker 1988). This can lead to an asymmetrical PN, but it is not clear that it can cause a butterfly PN. Second, a low mass companion might be evaporated while accreting from the envelope (Livio and Soker 1984). Third, if the separation between the companion and the core gets to be very small, new effects become important: (a) the envelope inner to the secondary orbit can reach corotation; (b) if the secondary is not too massive, it can collide with the core; (c) the secondary can influence the evolution of the shrinking envelope at the end of the RG phase. Soker (1989) discussed these last two effects and showed that they can shape the PN at an early time into having a high-density torus in the equatorial plane. All three effects can also form a large mass flow in the equatorial plane, eventually leading to a butterfly PN. Based on observational grounds, Mendez *et al.* (1988) suggested that a coalescence of the companion with the core can occur during the common envelope phase. They claim that such a common envelope, which can lead to mass loss during the first RG branch, and the coalescence can explain the single high surface gravity low-temperature stars in the center of the PNs 125 - 47 1 and 212 + 23 1.

Another possibility, which is discussed by Morris (1990), is the focusing of the outflow toward the equatorial plane by a detached companion. If a disk formed around the companion, it might collimate a flow to form the ansae observed in several PNs.

### b) Several Scenarios for the Formation of NGC 6826

The halo is not perfectly spherical (and this is not referring to the filaments and blobs which introduce deviation from symmetry on small scales). A spatially large, but very small-amplitude deviation from sphericity can be observed at the edge of the halo at two opposite locations along the direction of the major axis of the rim. This can be seen more clearly in the southeast direction as a bulge spanning  $\sim 55^\circ$ , protruding slightly from a complete circle boundary. More sensitive observations should elaborate more on this asymmetry.

In the following discussion we assume that a companion to the progenitor of NGC 6826 caused the asymmetry of the inner region. The almost spherically symmetric outer halo of NGC 6826 imposes constraints on the initial mass and separation of the companion to NGC 6826. If we accept that a deposition of angular momentum to the envelope leads to an asymmetrical wind, then the companion must have had a low initial mass or a small initial separation, or both. The asymmetrical inner region is then a result of one of the more violent effects mentioned above. We discuss a few plausible scenarios for the formation of NGC 6826 along these lines.

#### 1) Evaporation of the companion

A low mass companion, possibly a brown dwarf, spirals-in and accretes mass while the separation decreases. The brown dwarf is then evaporated and a high-density region made out of the evaporated companion is formed in the equatorial plane. Because of its very low mass the influence of the brown dwarf on the red giant envelope is very small, and an almost spherically symmetric wind at the initial stages of the common envelope evolution is expected.

An evolution of brown dwarfs inside a red giant envelope was calculated by Livio and Soker (1984). For the red giant model they used (Harpaz 1983) with outer radius of  $450 R_\odot$ , they find that brown dwarfs with initial mass less than  $\sim 10^{-2} M_\odot$  are evaporated inside the red giant envelope. Brown dwarfs with an initial mass of 0.01 and  $0.005 M_\odot$  are evaporated after  $\sim 4000$  and  $\sim 1800$  yr, respectively, both at only a few solar radii from the core. The maximum mass the above brown dwarfs reach by accretion are 0.055 and  $0.012 M_\odot$ , respectively. A Jupiter-like planet, with an initial mass of  $0.001 M_\odot$ , does not accrete much and is evaporated after  $\sim 1000$  yr. The maximum mass of the massive evaporated companions can be therefore a substantial fraction of the mass of the very inner elliptical region.

#### 2) Partial evaporation of the companion

Another possibility is that only a fraction of the companion is evaporated. This might be the case if the entire envelope is lost before the companion is completely evaporated. Another possibility is that the accreted mass is bound loosely to the brown dwarf, and is lost at the end of the common envelope phase. Hjellming and Taam (1990) find such a behavior in a  $1.25 M_\odot$  main-sequence star accreting from the envelope of a  $5 M_\odot$  RG. The companion accretes  $0.05 M_\odot$ , from which  $0.04 M_\odot$  is lost at later time and at smaller radii. This type of behavior leads to the same type of PN as in the first scenario but it leaves a binary at the center. A binary at the center of NGC 6826 was suggested based on infrared excess by Bentley (1989).

#### 3) Collision of the companion and the core

In this case mass can be blown away mainly in the equatorial plane in a way similar to that obtained in the collision of a  $0.2 M_\odot$  main-sequence star with a white dwarf in the numerical simulations of Soker *et al.* (1987). In an intermediate stage a geometrically thick disk around the core can be formed (Soker *et al.* 1987). Such a disk might collimate a wind from the central star, which eventually turns into a bright knot, an "ansa," at each side of the disk. A model with two opposite jets was suggested by Soker (1990) to explain the formation of ansae. This scenario leads to the same type of PN as the first two, it does not leave a binary at the center (assuming there is no third star in the system) and it has the advantage that jets, which explain the ansae, might be formed near the thick disk.

The inner region of NGC 6826 was found by Barker (1988) to contain low abundances of metals. He concludes that NGC 6826 was formed in a metal-poor region, and did not enhance the abundances by mixing with nuclear-processed material. Subsections 1 and 2 imply that a substantial fraction of the mass in the inner elliptical region is unprocessed material which originate from the brown dwarf. It is possible, therefore, that the low abundances of metals in the inner region of NGC 6826 is a consequence of the evaporation or destruction of the companion, and not of an absence of mixing. A serious problem with the companion explanation for the low abundances is that the abundances in the halo are lower than that of the inner region (Manchado and Pottasch 1989; Middlemass *et al.* 1989).

## VI. SUMMARY

CCD images of the planetary nebula NGC 6826 were taken in  $H\alpha$  and in the continuum. The density profile of the planetary nebula NGC 6826 was then deconvolved from its  $H\alpha$  emission measure, by assuming spherical symmetry. The last assumption might introduce some inaccuracy, especially in the inner axisymmetric region. By scaling the electron density to be  $1000 \text{ cm}^{-3}$  at 12 arcsec and assuming a distance of 1.54 kpc, the mass of the inner region  $r < 13$  arcsec was found to be  $\sim 0.15 M_\odot$ , and that of the entire visible nebula  $0.54 M_\odot$ . The possible formation of the dense shell at the edge of the nebula as a result of interaction with the ISM was discussed. It could have been formed by the ram pressure of the ISM on the expanding halo if the process took place when the halo was cold  $\sim 100$  K, and if the pressure of the ISM is  $n_I T_I \sim 10^4 \text{ cm}^{-3} \text{ K}$ . At the location of NGC 6826, 340 pc above the galactic plane, such a pressure can result from a hot medium together with a strong magnetic field. Another possibility is that the dense shell was formed from a short period of high mass-loss rate. Such a shell could have stayed thin if it were cold,  $\lesssim 100$  K, during most of its expansion. The formation of the spherical outer halo together with an elliptical inner region by mean of a companion to the progenitor was discussed. The evaporation of a low mass companion inside the RG envelope, or its collision with the core of the RG are consistent with the morphology of NGC 6826.

We thank Bruce Balick for sending us his data on NGC 6826 and Bruce Balick, Howard Bond, Kazimierz Borowski, Mark Whittle, and Mike Wise for helpful discussions.

## REFERENCES

- Balick, B. (1987). *Astron. J.* **94**, 671.
- Balick, B., Preston, H. L., and Icke, V. (1987). *Astron. J.* **94**, 1641 (BPI).
- Barker, T. (1988). *Astrophys. J.* **326**, 164.
- Bentley, A. F. (1989). In *Planetary Nebulae*, IAU Symposium No. 131, edited by S. Torres-Peimbert (Kluwer, Dordrecht), p. 312.
- Bodenheimer, P., and Taam, R. E. (1984). *Astrophys. J.* **280**, 771.
- Borkowski, K. J., Sarazin, C. L., and Soker, N. (1990). *Astrophys. J.* (in press).
- Chu, Y. H. (1989). In *Planetary Nebulae*, IAU Symposium No. 131, edited by S. Torres-Peimbert (Kluwer, Dordrecht), p. 105.
- Harpaz, A. (1983). *Mon. Not. R. Astron. Soc.* **210**, 633.
- Hippelein, H. H., Baessgen, M., and Grewing, M. (1985). *Astron. Astrophys.* **152**, 213.
- Hjellming, M. S., and Taam, R. E. (1990). Preprint.
- Jacoby, G. H., Quigley, R. J., and Africano, J. L. (1987). *Publ. Astron. Soc. Pac.* **99**, 672.
- Kwok, S. (1982). *Astrophys. J.* **258**, 280.
- Kwok, S., Purton C. R., and FitzGerald, P. M. (1978). *Astrophys. J.* **219**, L125.
- Livio, M., and Soker, N. (1984). *Mon. Not. R. Astron. Soc.* **208**, 763.
- Livio, M., and Soker, N. (1988). *Astrophys. J.* **329**, 764.
- Lockman, F. J. (1990). *Annu. Rev. Astron. Astrophys.* (in press).
- Manchado, A., and Pottasch, S. R. (1989). *Astron. Astrophys.* **222**, 219.
- Mendez, R. H., Groth, H. G., Husfeld, D., Kudritzki, R. P., and Herrero, A. (1988). *Astron. Astrophys.* **197**, L25.
- Middlemass, D., Clegg, R. E. S., and Walsh, J. R. (1989). *Mon. Not. R. Astron. Soc.* **239**, 1.
- Morris, M. R. (1990). In *From Miras to Planetary Nebulae: Which Path for Stellar Evolution?*, ed. M.-O. Mennessier.
- Perinotto, M. (1989). In *Planetary Nebulae*, IAU Symposium No. 131, edited by S. Torres-Peimbert (Kluwer, Dordrecht), p. 293.
- Soker, N. (1989). *Astrophys. J.* **340**, 927.
- Soker, N. (1990). *Astron. J.* (in press).
- Soker, N., Borkowski, K. J., and Srazin, C. L. (1990). In preparation.
- Soker, N., and Livio, M. (1989). *Astrophys. J.* **339**, 268.
- Soker, N., Regev, O., Livio, M., and Shara, M. M. (1987). *Astrophys. J.* **318**, 760.
- Torres-Peimbert, S. (1989). In *Planetary Nebulae*, IAU Symposium, No. 131, edited by S. Torres-Peimbert (Reidel, Dordrecht), p. 1.
- Volk, K., and Kwok, S. (1985). *Astron. Astrophys.* **153**, 79 (VK).

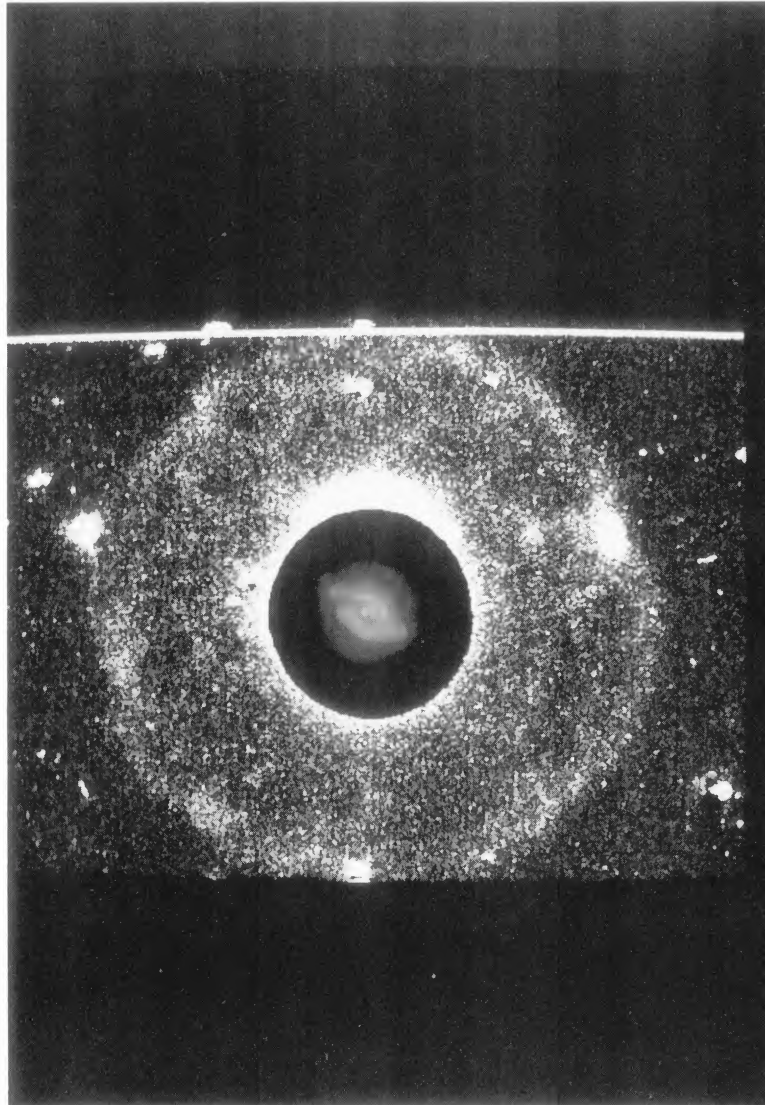


FIG. 1. Deep CCD image of NGC 6826. The contrast was stretched to show the outer halo. All pixel values inside a radius of 25 arcsec from the center have been rescaled to show detail of the inner region. North is up; east is to the right.

P. Plait and N. Soker (see page 1884)